

Towards a Complete Calculation of $\gamma\gamma \rightarrow 4f$.

Edward Boos[‡]
 Thorsten Ohl[¶]

Technische Hochschule Darmstadt
 Schloßgartenstr. 9
 D-64289 Darmstadt
 Germany

IKDA 97/16
 hep-ph/9705374
 May 1997

Abstract

We propose a general classification of all four fermion final states in $\gamma\gamma$ collisions at a future e^+e^- Linear Collider and discuss the relation of “signal” and “background” contributions in vector boson production. We utilize the results in a critical examination of the Higgs signal in sub-threshold W^+W^- pair production.

1 Introduction

A e^+e^- Linear Collider (LC) in the 500 GeV to 1 TeV range would provide exciting physics opportunities [1], complementary to the Large Hadron

^{*}On leave from Moscow State University.

[†]Supported by Deutsche Forschungsgemeinschaft (DFG).

[‡]email: boos@ifh.de

[§]Supported by Bundesministerium für Bildung, Wissenschaft, Forschung und Technologie (BMBF), Germany.

[¶]e-mail: Thorsten.Ohl@Physik.TH-Darmstadt.de

Collider (LHC) currently under construction. In addition to the e^+e^- annihilation mode, such a collider would allow to study physics in $e^-\gamma$ and $\gamma\gamma$ collisions as well. The photon beams can either be produced by Compton backscattering in a dedicated photon collider [2], but they are available, albeit with a softer spectrum, from beamstrahlung [3] and bremsstrahlung in any case. Therefore numerically precise and theoretically reliable calculations of $\gamma\gamma$ cross sections are required for unleashing the physics potential of such a machine.

Standard model predictions for on-shell gauge boson production in $\gamma\gamma$ collisions have been available for a long time in lowest order [4] and including electroweak radiative corrections [5]. However, the observed final state in these processes is not the gauge boson pair, but the four fermions that the gauge bosons decay into. The resonant diagrams that factorize into gauge boson production and decay do *not* form a gauge invariant subset. Therefore a more detailed investigation, including non-resonant “background” diagrams, is needed for obtaining theoretically consistent results. Complete calculations for $e^+e^- \rightarrow 4f$ have been performed in recent years (see [6] and references therein), but a similar analysis of $\gamma\gamma \rightarrow 4f$ is not available yet.

For some gauge invariant subsets of the diagrams contributing to $\gamma\gamma \rightarrow 4f$, first numerical results in the region above the W^+W^- threshold have been published recently [7, 8]. These studies have focused on numerical calculations of cross sections for specific final states and have not attempted a complete investigation of $\gamma\gamma \rightarrow 4f$. There have also been earlier analytical calculations of the high energy asymptotics of $\gamma\gamma \rightarrow \ell^+\ell^-e^+e^-$ in QED [9]. In order to pave the road for a more systematic treatment, we will give a classification of all gauge invariant subsets for $\gamma\gamma \rightarrow 4f$ in section 2.

Recently, the search for the intermediate mass Higgs in the reaction $\gamma\gamma \rightarrow H \rightarrow W^+W^-$ below threshold, i.e. with one off-shell W has been discussed in [10]. This scenario will provide us with an application of our classification. It is obvious that in this range ($\sqrt{s} \approx M_H \lesssim 2M_W$), the on-shell diagrams in figure 1 can serve as a rough estimate only and that a more complete analysis is required. In section 3 we will present numerical results for this process and we will discuss their phenomenological implications.

We will conclude with an outlook on the construction of a complete Monte Carlo event generator for $\gamma\gamma \rightarrow 4f$, which is in progress.

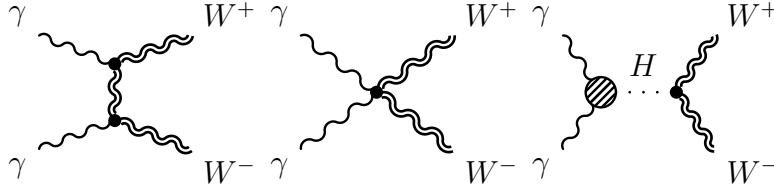


Figure 1: On-shell W^+W^- production and Higgs signal.

2 Classification of Feynman Diagrams

We start with a classification of all Feynman diagrams contributing to four fermion production in $\gamma\gamma$ collisions. This classification has to be done from two perspectives: on one hand we have to investigate the different topologies and singularity structures for disentangling signals from backgrounds and for constructing an efficient Monte Carlo event generator. On the other hand, we have to classify the flavor structure of the final states and the gauge invariant subsets of diagrams corresponding to them. In this classification we will use the analogue of the established notation proposed for $e^+e^- \rightarrow 4f$ in [11].

We will perform the classification for massless fermions and in unitarity gauge first. Later we will discuss the modifications for massive fermions and for R_ξ gauge.

2.1 Topologies and Singularities

The Feynman diagrams for $\gamma\gamma \rightarrow 4f$ have six different topologies, which are depicted in figure 2. All diagrams can be derived from these six topologies by charge conjugation and permutation of final state fermions.

Each of these topologies corresponds to a particular singularity structure and will be dominant in different regions of phase space: Q and D have two resonant gauge boson propagators, while T , S and B have a single resonant gauge boson. The multi-peripheral contribution M has no resonant gauge bosons at all. An efficient multi channel event generator will use these six topologies as subchannels for mapping kinematical singularities.

2.2 Final States and Gauge Invariant Subsets

While the unravelling of the singularity structures presented in the previous section is essential for the construction of a Monte Carlo event generator, the

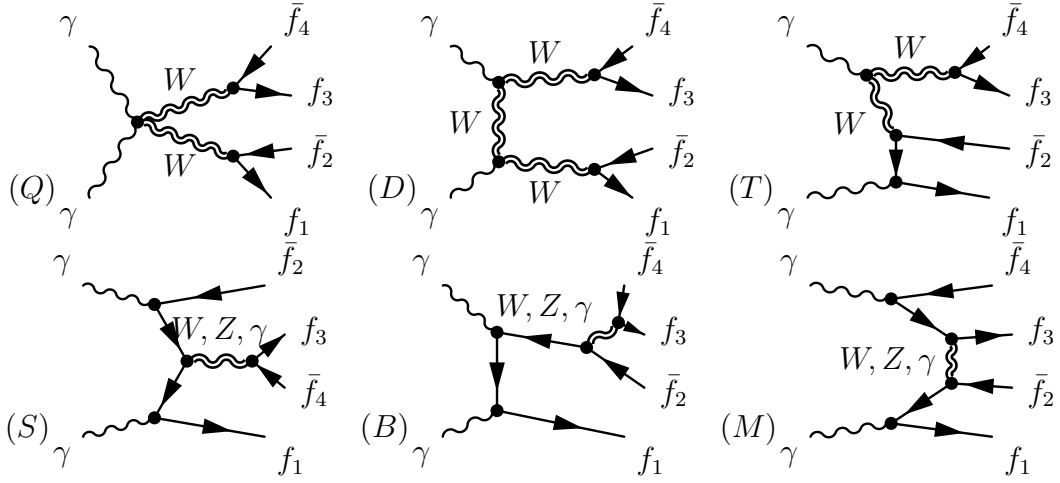


Figure 2: Topologies with a quartic gauge coupling (Q), with two triple gauge couplings (D), with one triple gauge coupling (T), with single vector boson production (S), with gauge boson bremsstrahlung (B) and multi-peripheral diagrams (M).

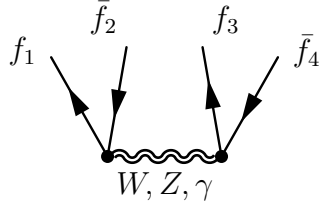


Figure 3: Amplitude for $|0\rangle \rightarrow f_1 \bar{f}_2 f_3 \bar{f}_4$, from which all diagrams are derived.

classification of the gauge invariant subsets is more conveniently performed from a different point of view.

Since the photon couplings are diagonal in flavor space, the flavor structure of the four fermion final states can be investigated easily by looking at the amplitude for $|0\rangle \rightarrow f_1 \bar{f}_2 f_3 \bar{f}_4$ (see figure 3). The gauge invariant¹ subsets of diagrams are then obtained by hooking two photons to the charged propagators in all possible ways.

For two generations and a diagonal CKM matrix, there are altogether 45 different four fermion final states in $\gamma\gamma$ collisions. Twelve of these are six

¹Gauge invariant for vanishing gauge boson width. We are not yet concerned with the intricate interplay of resummation and gauge invariance [12].

Class		Final States				3 rd Gen.
<i>CC13</i>	l	$e^- \bar{\nu}_e \mu^+ \nu_\mu$	$e^+ \nu_e \mu^- \bar{\nu}_\mu$			+4
<i>CC21</i>	sl	$e^- \bar{\nu}_e u d$	$e^+ \nu_e \bar{u} d$	$e^- \bar{\nu}_e c \bar{s}$	$e^+ \nu_e \bar{c} s$	
		$\mu^- \bar{\nu}_\mu u d$	$\mu^+ \nu_\mu \bar{u} d$	$\mu^- \bar{\nu}_\mu c \bar{s}$	$\mu^+ \nu_\mu \bar{c} s$	+10
<i>CC31</i>	h	$u d \bar{c} s$	$d \bar{u} c \bar{s}$			+4

Table 1: The 12 *CCn* final states. Including a third generation increases the count to 30. In this and the following tables, we tag leptonic, semileptonic and hadronic final states with ‘l’, ‘sl’ and ‘h’ respectively.

Class		Final States				3 rd Gen.
<i>NC06</i>	l	$\nu_e \bar{\nu}_e \mu^- \mu^+$	$\nu_\mu \bar{\nu}_\mu e^- e^+$			+4
<i>NC06</i>	sl	$\nu_e \bar{\nu}_e u \bar{u}$	$\nu_e \bar{\nu}_e d \bar{d}$	$\nu_e \bar{\nu}_e c \bar{c}$	$\nu_e \bar{\nu}_e s \bar{s}$	
		$\nu_\mu \bar{\nu}_\mu u \bar{u}$	$\nu_\mu \bar{\nu}_\mu d \bar{d}$	$\nu_\mu \bar{\nu}_\mu c \bar{c}$	$\nu_\mu \bar{\nu}_\mu s \bar{s}$	+10
<i>NC20</i>	l	$e^- e^+ e^- e^+$	$\mu^- \mu^+ \mu^- \mu^+$			+1
<i>NC20</i>	h	$u \bar{u} u \bar{u}$	$d \bar{d} d \bar{d}$	$c \bar{c} c \bar{c}$	$s \bar{s} s \bar{s}$	+2
<i>NC40</i>	l	$e^- e^+ \mu^- \mu^+$				+2
<i>NC40</i>	sl	$e^- e^+ u \bar{u}$	$e^- e^+ d \bar{d}$	$e^- e^+ c \bar{c}$	$e^- e^+ s \bar{s}$	
		$\mu^- \mu^+ u \bar{u}$	$\mu^- \mu^+ d \bar{d}$	$\mu^- \mu^+ c \bar{c}$	$\mu^- \mu^+ s \bar{s}$	+10
<i>NC40</i>	h	$u \bar{u} s \bar{s}$	$u \bar{u} c \bar{c}$	$d \bar{d} s \bar{s}$	$d \bar{d} c \bar{c}$	+4

Table 2: The 29 *NCn* final states. Including a third generation increases the count to 62.

pairs of charge conjugate states. The third generation will add 53 final states, which are trivial replicas of final states appearing in the two generation case. Therefore we will restrict our discussion to the case of two generations.

Obviously, the sets $f_1 \bar{f}_2 f_3 \bar{f}_4$ fall into three classes. The first class contains 12 final states (*CCn*, see table 1) where the two pairs exchange a W . They consist of two pairs of particles with the anti-particle of their partner from the weak isospin doublet. The second class contains 29 final states (*NCn*, see table 2) that exchange a neutral gauge boson, Z or γ . They consist of two pairs of particles with their antiparticles. Finally there are four final states (*mixn*, see table 3) that can exchange both charged and neutral gauge bosons.

Counting the number of diagrams for processes in each class is simple.

Class		Final States	3 rd Gen.
<i>mix19</i>	l	$e^-e^+\nu_e\bar{\nu}_e \quad \mu^-\mu^+\nu_\mu\bar{\nu}_\mu$	+1
<i>mix71</i>	h	$u\bar{u}dd \quad c\bar{c}s\bar{s}$	+1

Table 3: The 4 *mixn* final states. Including a third generation increases the count to 6.

n_c	CC	NC	mix
0	—	—	—
1	—	—	—
2	$CC13$	$NC06$	$mix19$
3	$CC21$	—	—
4	$CC31$	$NC40$	$mix71$
4'	—	$NC20$	—

Table 4: Counting diagrams.

Obviously, it can only depend on the number n_c of charged fermions. For the CCn case, there are $n_c + 1$ charged propagators to attach the first photon to and consequently $n_c + 2$ for the second photon. Adding the single diagram with a $W^+W^-\gamma\gamma$ vertex, we find

$$N_{CC} = n_c^2 + 3n_c + 3 \quad (n_c > 0). \quad (1)$$

From charge conservation, only the cases $n_c = 2, 3, 4$ are realized, leading to the sets $CC13$, $CC21$ and $CC31$, respectively.

In the NCn case, there are n_c charged propagators for the first photon and $n_c + 1$ for the second. Taking into account that both Z and γ can be exchanged for $n_c = 4$, we can write

$$N_{NC} = \frac{n_c^2(n_c + 1)}{2} \quad (n_c \in \{0, 2, 4\}). \quad (2)$$

Only the cases $n_c = 2, 4$ are realized, leading to the sets $NC06$ and $NC40$. For final states involving identical particles, the $NC40$ degenerates to a $NC20$.

Finally, the $CC13$ and $NC06$ can be combined to $mix19$ and $CC31$ and $NC40$ can be combined to $mix71$.

Class		Q	T	D	S	B	M
<i>CC13</i>	l	1	4	2	0	4	2
<i>CC21</i>	sl	1	6	2	2	6	4
<i>CC31</i>	h	1	8	2	4	8	8
<i>NC06</i>	l/sl	0	0	0	2	4	0
<i>NC20</i>	l/h	0	0	0	4	8	8
<i>NC40</i>	l/sl/h	0	0	0	8	16	16
<i>mix19</i>	l	1	4	2	2	8	2
<i>mix71</i>	h	1	8	2	12	24	24

Table 5: The eight classes of diagrams in $\gamma\gamma \rightarrow 4f$ and the corresponding topologies. Note that $NC40 = 2 \cdot NC20$, $mix19 = NC06 + CC13$ and $mix71 = NC40 + CC31$.

It is now a straightforward combinatorial exercise to determine the number of Feynman diagrams from each topology contributing for a specific final state. The result is shown in table 5.

2.3 Massive Fermions

The modifications for massive fermions in unitarity gauge are trivial: iff all four fermions are massive, the sets $NC20$ and $NC40$ are augmented by Higgs exchange diagrams to $NC30$ and $NC60$. All final states corresponding to the set $NC06$ contain neutrinos (see table 2) and remain unaffected. The charged current final states remain unaffected by the Higgs at tree level as well.

2.4 R_ξ Gauge

In a R_ξ gauge, additional diagrams involving the charged and neutral Goldstone bosons ϕ^\pm, ϕ^0 have to be taken into account. Since the couplings of the Goldstone bosons are proportional to the masses of the participating particles, only the diagram D' depicted in figure 4 has to be added for massless fermions in the final state.

For massive fermions, the situation is more involved, but it can be summarized in the rule that each massive gauge boson that is connected to massive particles at *both* ends can be replaced by its corresponding Goldstone boson

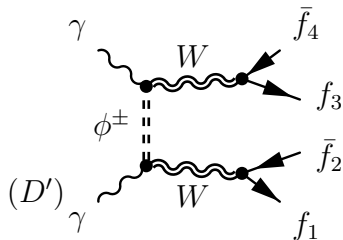


Figure 4: Sole additional diagram in R_ξ gauge for massless fermions.

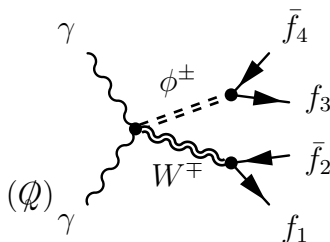


Figure 5: Exception to the rule that gauge bosons can be replaced by their corresponding Goldstone bosons individually. This diagram and its charge conjugate are *absent*.

individually. The only exception to this rule is that there is no $W^\mp \phi^\pm \gamma \gamma$ vertex. Therefore the diagram \mathcal{Q} depicted in figure 5 and its charge conjugate are *absent*.

3 Cross Sections

For a numerical illustration of the importance of “background” diagrams, we present results for cross sections for two CCn final states. The calculations have been performed by means of the **CompHEP** system [13]. We present the results as a function of the $\gamma\gamma$ invariant mass $\sqrt{s'}$.

3.1 CC13: $e^+ \mu^- \bar{\nu}_\mu \nu_e$

This state has a very clean signature: a muon, a positron, missing energy and no other activity in the detector. It is the smallest gauge invariant subset containing resonant W pair production. Nevertheless, it involves all topologies except one. Cross sections for this final state have been calculated

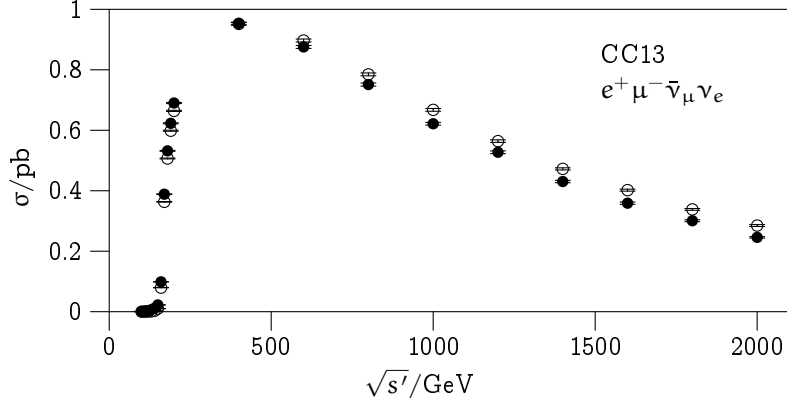


Figure 6: *CC13* cross section (full circles) and signal contribution (open circles), after the canonical LC cuts: $E_{\text{lepton}} > 1 \text{ GeV}$, $\theta_{\text{lepton}} > 10 \text{ deg}$, $E_{\text{jet}} > 3 \text{ GeV}$, $\theta_{\text{jet}} > 5 \text{ deg}$, $\theta_{\text{lepton,lepton}'} > 5 \text{ deg}$, $\theta_{\text{lepton,jet}} > 5 \text{ deg}$ and $m_{\text{jet,jet}'} > 10 \text{ GeV}$. The 1sd error bars are shown, unless they are smaller than the thickness of the lines.

earlier in [7].

Figure 6 shows the total cross section for *CC13* with the canonical cuts for the DESY/ECFA Linear Collider study (our results agree with [7] in their cuts). Since this final state includes two neutrinos, no invariant mass cut can be applied to suppress the “background”. Clearly, the cross section is dominated above threshold by the “signal”. However, an excess in this channel would be a signal for rather exotic flavor changing “new physics”. Therefore, the standard model contribution has to be known to high accuracy, including “background” contributions.

3.2 CC21: $e^- \bar{\nu}_e u \bar{d}$

The *CC21* diagrams have been calculated before in [8]. Figure 7 shows the total cross section for *CC21* with the canonical cuts for the DESY/ECFA Linear Collider study (using the cuts of [8] we find agreement again). Here we can also apply an invariant mass cut for the two jets. Such a cut will be used in the experiment for event selection and it will suppress background diagrams. In figure 7 we have applied the cut $M_W - 10 \text{ GeV} \leq \sqrt{(p_1 + p_2)^2} \leq M_W + 10 \text{ GeV}$ to both signal and full cross section. Again, the cross section

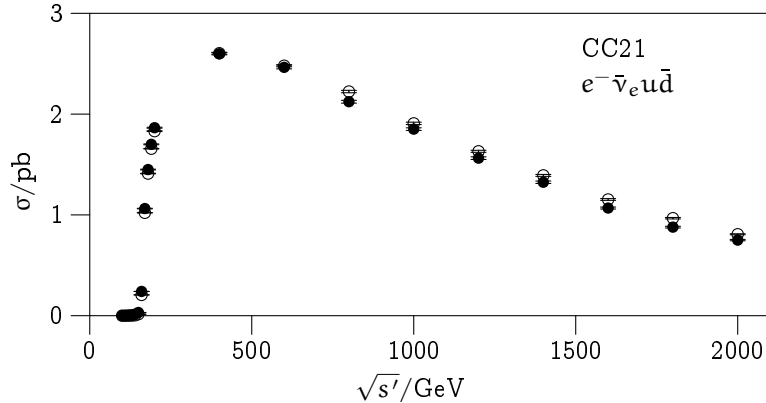


Figure 7: *CC21* cross section (full circles) and signal contribution (open circles), after the canonical NLC cuts. An invariant mass cut of $M_W - 10\text{GeV} \leq \sqrt{(p_1 + p_2)^2} \leq M_W + 10\text{GeV}$ has been applied to both cross sections.

is dominated above threshold by the “signal”, but for detailed studies of the vector boson couplings, the “background” contributions cannot be neglected.

3.3 Sub-Threshold Cross sections

In figure 8 we have enlarged the region below the W^+W^- threshold. In this region, which can be important in the search for an light intermediate mass Higgs, the cross section is several times larger than the prediction from the “signal diagrams” only. Therefore, the signal to background ratios predicted in studies based on “signal diagrams” only (cf. [10]) have to be reduced considerably. Nevertheless, since the standard model contributions can be calculated completely, this is only a technical obstacle pointing to the need for complete calculations.

4 Conclusions

We have proposed a complete classification of four fermion final states in $\gamma\gamma$ collisions. As an application, we have demonstrated the need for full, gauge invariant calculations for obtaining reliable predictions below the W^+W^- threshold. The restriction of calculations to the “signal diagrams” is not suf-

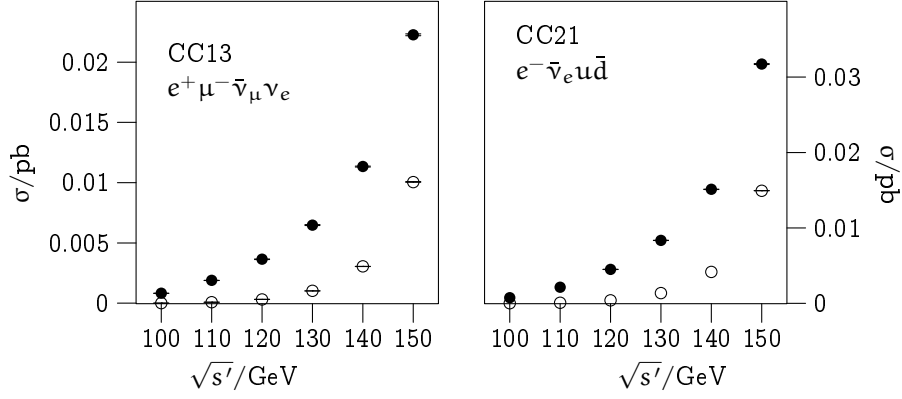


Figure 8: Sub-threshold cross section (full circles) and signal contribution (open circles).

ficient. Therefore the signal to background ratios presented in [10] turn out to be far too optimistic. Nevertheless, once a complete calculation is available, the potential of the Linear Collider for the intermediate mass Higgs can be realized.

While the results presented in this note correspond to full calculations and are gauge invariant, they can only be a first step. A Monte Carlo event generator will be required for more detailed experimental studies. Only such a tool will allow the efficient simulation of $\gamma\gamma \rightarrow 4f$ for arbitrary experimental cuts.

The helicity amplitudes and the phase space for massless fermions are relatively simple. Therefore, the construction of a Monte Carlo event generator for $\gamma\gamma \rightarrow 4f$ with massless fermions will be the natural next step [14] towards a complete calculation.

References

- [1] JLC Group, KEK Report 92-16; NLC ZDR Design Group and NLC Physics Working Groups, SLAC-Report-485; NLC ZDR Design Group, SLAC-Report-474; H. Murayama and M. E. Peskin, SLAC-PUB-7149, to appear in *Ann. Rev. Nucl. Part. Sci.*; P. Zerwas, DESY 94-001-REV.

- [2] I. Ginzburg, G. Kotkin, V. Serbo, and V. Telnov, *Pisma ZhETF* **38**, 514 (1981); I. Ginzburg, G. Kotkin, V. Serbo, and V. Telnov, *Nucl.Inst. Meth.* **205**, 74 (1983).
- [3] P. Chen and R. J. Noble, SLAC-PUB-4050.
- [4] V. Kompaniec, *Yad. Fiz.* **12**, 826 (1970); O. Sushkov, V. Flambaum, and I. Khriplovich, *Yad. Fiz.* **20**, 1016 (1974); E. Yehudai, *Phys. Rev.* **D44**, 3434 (1991); S. Choi and F. Schrempp, *Phys. Lett.* **B272**, 149 (1991); E. Boos and G. Jikia, *Phys. Lett.* **B275**, 164 (1992); G. Belanger and F. Boudjema, *Phys. Lett.* **B288**, 210 (1992).
- [5] A. Denner, S. Dittmaier, and R. Schuster, *Nucl. Phys.* **B452**, 80 (1995).
- [6] W. Beenakker *et al.*, in *Physics at LEP2, Vol. 1*, edited by G. Altarelli, T. Sjöstrand, and F. Zwirner, CERN 96-01, p. 79; D. Bardin *et al.*, in *Physics at LEP2, Vol. 2*, edited by G. Altarelli, T. Sjöstrand, and F. Zwirner CERN 96-01, p. 3.
- [7] G. Couture, *Phys. Rev.* **D44**, 2755 (1991); S. Moretti, [hep-ph/9606225](#).
- [8] S. Moretti, *Nucl. Phys.* **B484**, 3 (1997); M. Baillargeon, G. Belanger, and F. Boudjema, ENSLAPP-A-635/97, FISIST/2-97/CFIF, [hep-ph/9701368](#).
- [9] E. Kuraev, A. Schiller, and V. Serbo, *Nucl. Phys.* **B256**, 189 (1985).
- [10] I. Ginzburg and I. Ivanov, Technical report, Institute of Mathematics, Novosibirsk, [hep-ph/9704220](#).
- [11] D. Bardin *et al.*, *Nucl. Phys. (Proc. Suppl.)* **37B**, 148 (1994).
- [12] E. Argyres *et al.*, *Phys. Lett.* **B358**, 339 (1995); W. Beenakker *et al.*, NIKHEF-96-031, [hep-ph/9612260](#).
- [13] E. Boos *et al.*, in *Proceedings of the XXVIth Rencontre de Moriond*, edited by I. T. T. Van (Editions Frontiers, Paris, 1991), p. 501; E. Boos *et al.*, SNUTP-95-116, [hep-ph/9503280](#); P. Baikov *et al.*, in *Proceedings of the Xth Workshop on High Energy Physics and Quantum Field Theory*, edited by B. Levtchenko and V. Savrin (Moscow, 1996), p. 101, [hep-ph/9701412](#).

[14] E. Boos and T. Ohl, in preparation.